Geophysical Journal International

Geophys. J. Int. (2015) **202,** 419–423
GJI Seismology

doi: 10.1093/gji/ggv147

EXPRESS LETTER

Report on a characteristic oscillation about 38 mHz (26 s) in northeastern Japan following surface wave of the 2011 Tohoku megathrust earthquake

Yuta Mitsui[1] and Kosuke Heki[2]

[1] *Department of Geosciences, Shizuoka University,* 836, *Ohya, Suruga-ku, Shizuoka* 422–8529, *Japan. E-mail: mitsui.yuta@shizuoka.ac.jp*
[2] *Department of Natural History Sciences, Hokkaido University, N*10*W*8, *Kita-ku, Sapporo* 060–0810, *Japan*

Accepted 2015 March 31. Received 2015 March 31; in original form 2015 February 15

SUMMARY

We try to detect an unidentified signal from the surface motion at northeastern Japan immediately after the 2011 Tohoku earthquake. A focused frequency range is 10–100 mHz (10–100 s). We find a peaky signal with frequency of about 38 mHz (26 s) based on the horizontal-to-vertical (H/V) spectral ratio using the high-rate GNSS data at 382 GEONET stations. We are not able to identify locality of the signal. The signal appears several minutes after the passing of surface wave fronts. The duration of the signal is about 2 min. Since the origin of the 38 mHz signal is unlikely to be local hydrologic tremors, tectonic tremors, or the tsunami, we speculate that the 38 mHz signal originates from a kind of a characteristic oscillation of Northeastern Japan triggered by the 2011 Tohoku earthquake. A normal-mode simulation implies that high-order radial overtones could create the signal with a spherically-layered velocity structure, however, the detailed mechanism of the signal still remains a mystery.

Key words: Satellite geodesy; Transient deformation; Broad-band seismometers; Surface waves and free oscillations; Asia.

1 INTRODUCTION

The 2011 Tohoku megathrust earthquake at northeastern Japan near the Japan trench ruptured a wide region of the plate interface between the Pacific Plate and the Okhotsk Plate. The moment magnitude of the Tohoku earthquake was over 9 (e.g. Nettles *et al.* 2011), causing significant seismic wave on the Japan islands (e.g. Furumura *et al.* 2011). The radiated seismic wave dynamically triggered small earthquakes (Miyazawa 2011; Gonzalez-Huizar *et al.* 2012) and local landslides (Miyagi *et al.* 2011). Other triggered phenomena might occur after the 2011 Tohoku earthquake without being discovered.

Global Navigation Satellite System (GNSS) can detect surface deformation in a wide range of frequency from 0 to 50 Hz (e.g. Ge *et al.* 2000; Larson *et al.* 2003; Genrich & Bock 2006; Avallone *et al.* 2011). A GNSS array by Geospatial Information Authority of Japan, GEONET, succeeded in detecting seismic wave precisely (Grapenthin & Freymueller 2011; Psimoulis *et al.* 2014) and Earth's free oscillation (Mitsui & Heki 2012). Mitsui & Heki (2012) showed that data stacking over several hundred stations illuminated the small signals of the Earth's free oscillation in a frequency range of 0.5–4 mHz (250–2000 s).

Here, we try to detect 'unidentified' signals from the surface motion immediately after the 2011 Tohoku earthquake. In particular, we focus on a frequency range of 10–100 mHz (10–100 s) in which the high-rate GNSS has good signal-to-noise ratios (Elosegui *et al.* 2006).

2 METHODS

We use GNSS time-series data analysed by the kinematic precise point positioning method (e.g. Kouba & Heroux 2001), provided by the Geospatial Information Authority of Japan (GSI) via Nippon GPS Data Services Company (NGDS) and the VERIPOS/APEX service using the RTnet software (GPS Solutions). The sampling period Δt is 1 s. The absolute coordinates of the GNSS stations were estimated on the basis of the precise ephemeris and clock with the ionospheric-free linear combination of dual-frequency carrier-phase observations.

Errors in the ephemeris or clock, and tropospheric path delay of radio waves might contaminate the analysed data for the land displacement, but there were no organized reports about such an error in the period immediately after the 2011 Tohoku earthquake, to our knowledge. Besides, we can neglect characteristic oscillations of the GNSS antennas since its natural frequency is certainly higher than the sampling frequency of 1 Hz (note that 1 Hz is roughly as large as natural frequencies of buildings).

We focus on the 1-Hz data immediately after the 2011 Tohoku earthquake at the GEONET stations in NE Japan (Fig. 1).

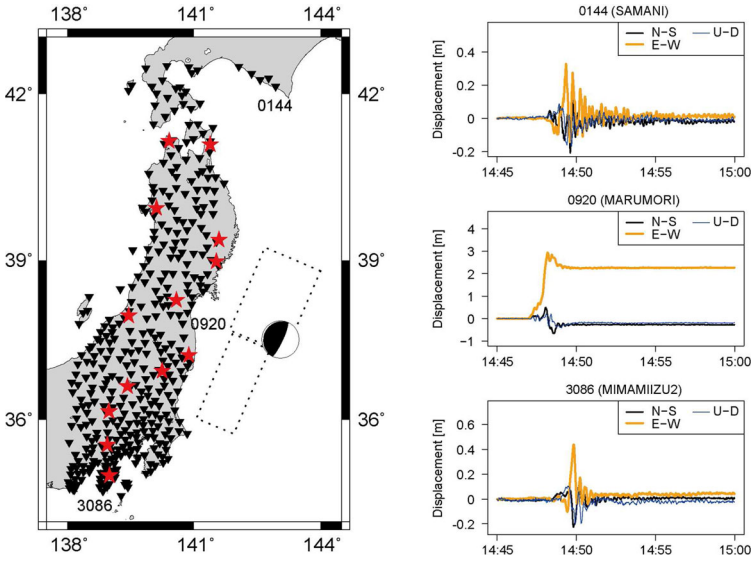

Figure 1. We use GNSS time-series data at 382 GEONET stations (solid triangles) and seismometer data at 13 F-net stations (red stars) in NE Japan, near the source region of the 2011 Tohoku earthquake. The GCMT solution (Nettles *et al.* 2011) is represented by the beach-ball symbol. The ruptured area estimated by Geospatial Information Authority of Japan (2011) is also represented by the dashed squares. The right-hand figures show the observed three-component displacement data at selected GEONET stations. The 0144 station is at (142.935°E, 42.131°N), the 0920 station is at (140.728°E, 37.825°N), and the 3086 station is at (138.838°E, 34.610°N).

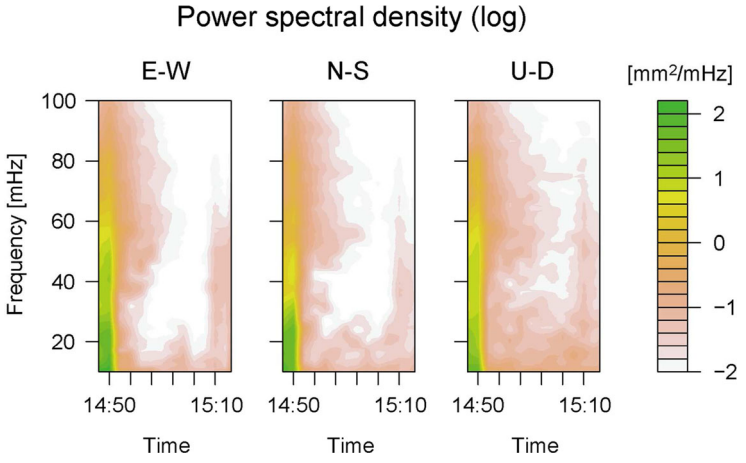

Figure 2. Power spectral densities in three components (north–south, east–west and up–down) over the 382 GNSS stations after the occurrence of the 2011 Tohoku earthquake (14:46). The length of the time window for the running spectrum is 6 min and the increment of the window shift is 2 min.

The 2011 Tohoku earthquake occurred around 14:46 (JST) on March 11. Since the large wave groups of the surface waves had almost passed through the GEONET stations around 14:50 (Grapenthin & Freymueller 2011), we mainly consider the data after 14:51 (JST).

In order to obtain anonymous signals, we first remove linear trends from all the time-series data and then compute their power spectral densities. The power spectral density P for each data is given by $|D|^2/T$, where D is the data in the frequency domain and T is the measurement period. We obtain D by the discrete Fourier transform using an FFT method (Singleton 1979) with the Hann window (Blackman & Tukey 1959):

$$D(k) = \Delta t \sum_{m=0}^{N-1} d(m)\{0.5 - 0.5\cos[2\pi m/(N-1)]\} \times \exp(-2\pi i k m/N),$$

where Δt is the sampling period (1 s), N is number of the time-series with zero padding, and d is the original (time-series) data.

3 RESULTS

We first checked the power spectral density at each station but the spectra were rather complex and oscillating. Following our previous study (Mitsui & Heki 2012), we stack the data over many stations to extract some signals. Hence we obtain median values of the power spectral densities over all the stations (382 stations) for three components (north–south, east–west and vertical). Fig. 2 shows the power spectral densities after the occurrence of the main shock (14:46). In all the components, the spectral densities have maximal values immediately after the main shock and decay until about 15:10. The increases in the densities around 15:10 are caused by an $M7$-class aftershock, which were the first large aftershock of the Tohoku earthquake (e.g. Asano *et al.* 2011). There does not seem other notable signal in Fig. 2.

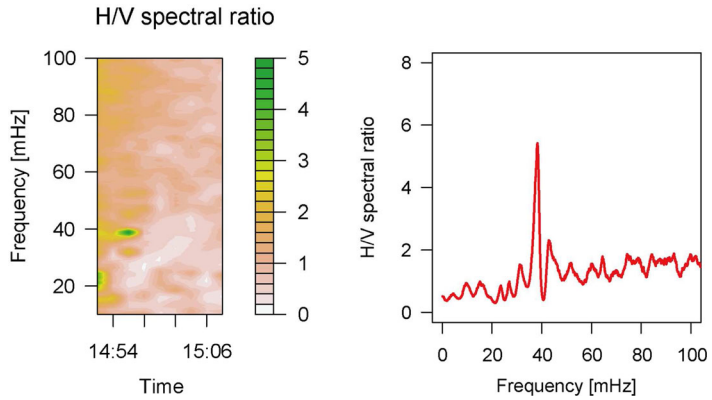

Figure 3. The H/V spectral ratio from the median value over the 382 GNSS stations. The left-hand figure is the running spectrum, and the right-hand figure is the simple spectrum for a period of 14:51–15:00.

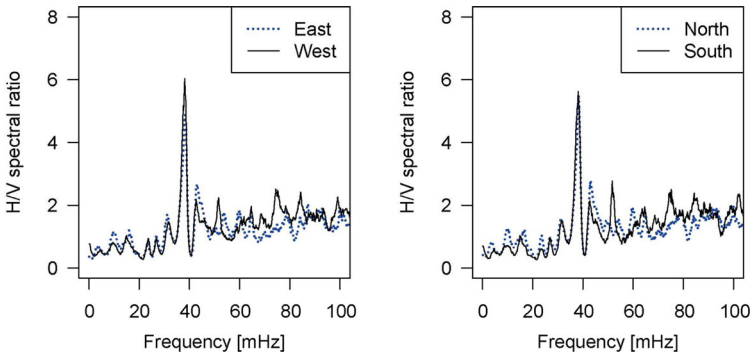

Figure 4. The H/V spectral ratio from parts of the GNSS data. The left-hand figure shows the median H/V ratios for the 174 eastern stations (>140.0°E) and the 208 western stations (<140.0°E). The right-hand figure presents the median H/V ratios for the 193 northern stations (>37.0°N) and the 189 southern stations (<37.0°N).

Next, we take the horizontal-to-vertical (H/V) spectral ratio (Nakamura 1989; Bonnefoy-Claudet *et al.* 2006), which has been generally used to evaluate local site effects relating to the fundamental mode of Rayleigh waves in a frequency range higher than 1 Hz.

Fig. 3 presents the results. We find an isolated peak around 38 mHz (26 s) in a period about 14:55–14:57. Such a sharp spectral peak following the 2011 Tohoku earthquake has not been reported before. Apparently, the larger spectral density in E-W component and the smaller density in U-D component constructed the larger H/V signal. The extent of the peak concentrates in a range of 36–40 mHz. This range differs from the second Airy phase (about 20 mHz) of the fundamental mode of Rayleigh waves for isotropic PREM (Widmer-Schnidrig & Laske 2007).

In order to check locality of the signal, we divide the observation area into Eastern–Western zones (the boundary is 140.0°E) or northern–southern zones (the boundary is 37.0°N). Fig. 4 shows the results and reveals that the typical signal around 38 mHz appears over the whole observation area.

4 DISCUSSION

We only used the GNSS displacement data for analysing the post-seismic deformation of the 2011 Tohoku earthquake. Since there are many seismometer stations on Japan, we also use continuous time-series data by the VSE-355G2 and VSE-355G3 strong-motion seismometers to compare with the GNSS results. The distribution of the seismometer stations of the F-net (by National Research Institute for Earth Science and Disaster Prevention) is illustrated in Fig. 1. We analyse the seismometer data by the same method as the GNSS data excluding the following points. First, we must correct the instrument responses of the seismometers in a low frequency range using complex transfer function in the Fourier domain. Next, the sampling rate Δt for the seismometer is 0.01 s.

Fig. 5 shows the comparative results of the GNSS and the strong-motion seismometer. From the left-hand figure, we find that the 38 mHz peaky signal also exists during 14:51–15:00 in the seismometer data, but several other peaky signals appear especially in the lower frequency range possibly caused by the less accuracy of the seismometer data for such a frequency range (Clinton 2004) or the smaller numbers of the seismometer stations. To check this point, in the right-hand figure, we compare between the GNSS data at one station and the seismometer data at a close station. We focus on a period of 15:09–15:11, which includes a seismic wave by the *M*7-class aftershock occurred about 15:08 (e.g. Asano *et al.* 2011). We found that the GNSS and seismometer data are better consistent. It implies that the several peaky signals only appeared in the seismometer data during 14:51–15:00 are owing to the smaller numbers of the seismometer stations.

The origin of the 38 mHz signal is now under discussion. We were not able to identify the locality of the signal. Thus the signal does not originate from local hydrologic tremors (Nishida & Shiomi 2012). Extensively triggered tectonic tremors are also unlikely to operate as the source of the signal, since the occurrence of the tectonic tremors has been rarely reported in Northeastern Japan (e.g. Beroza & Ide 2011). One may consider that the huge tsunami

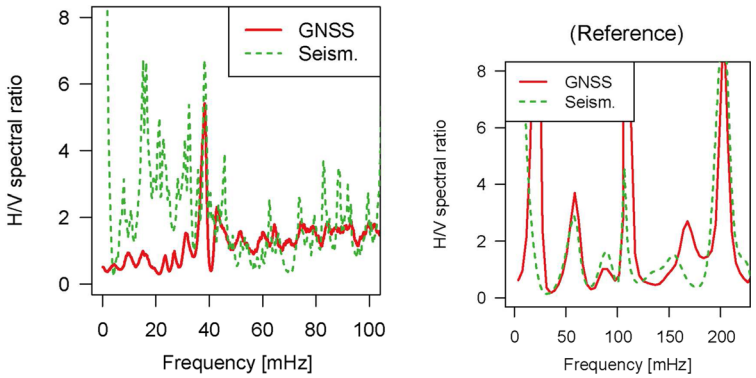

Figure 5. Left-hand figure: the median H/V spectral ratios during 14:51–15:00 from the GNSS data over the 382 stations and the strong-motion seismometer data over the 13 stations. The thick red line represents the GNSS result (same as Fig. 2). The green broken line represents the strong-motion seismometer result. Right-hand figure: comparison between the GNSS data and the strong-motion seismometer data at close stations during 15:09–15:11, including a seismic wave by an $M7$-class aftershock, for reference. The GNSS station is at (140.132°E, 39.936°N), and the seismometer station is at (140.111°E, 39.956°N).

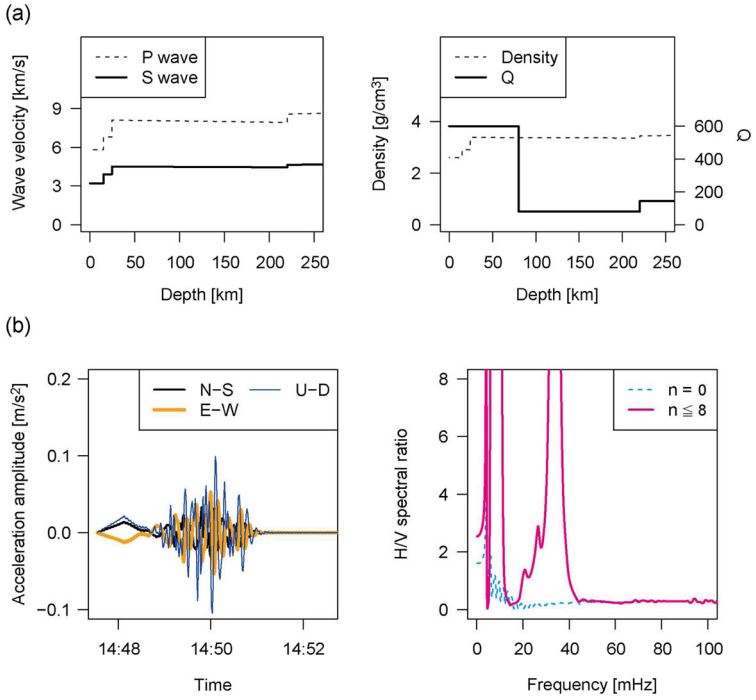

Figure 6. (a) Depth-dependent structures of the *P*-wave velocity, the *S*-wave velocity, the density, and the quality factor Q. We refer to the Preliminary Reference Earth Model (Dziewonski & Anderson 1981) without anisotropy. The shallowest ocean part in the original model is filled with the solid crust part. (b) The left-hand figure shows the three-component time-series data for the 2011 Tohoku earthquake at (140°E, 39°N), calculated by the normal-mode summation including the overtones. The right-hand figure illustrates the calculated H/V ratios in the period of 14:51–15:00. The blue broken line represents the result for only fundamental mode ($n = 0$). The pink line represents the result with the overtones ($n \leq 8$).

approaching the coast of Japan caused the 38 mHz signal. However, this mechanisms seems also improbable because the tsunami load mainly induces vertical land deformation (e.g. Mitsui & Heki 2013) leading to small H/V ratios. Another possibility is the effect of a thick column of water near the trench (Nakanishi 1992; Yomogida *et al.* 2002; Noguchi *et al.* 2013). Noguchi *et al.* (2013) demonstrated the importance of the water layer on the propagation of the Rayleigh wave around a period of 10–15 s near the Japan trench. This mechanism may affect the land deformation after the 2011 Tohoku earthquake, but the period range seems slightly different from that of the observed peaky signal in this study.

By contrast, a more general mechanism independent of locality may explain the 38 mHz signal. For this purpose, we compute synthetic seismograms of the 2011 Tohoku earthquake by summation of normal modes. We input the GCMT solution (Nettles *et al.* 2011) and the Preliminary Reference Earth Model (Dziewonski & Anderson 1981) into the MINEOS package (Masters *et al.* 2011). The shallow ocean part in the preliminary reference earth model is filled with the solid crust part. Fig. 6(a) shows the spherically layered structures of the *P*-wave velocity, the *S*-wave velocity, the density, and the quality factor Q, above 250 km depth.

We calculate the seismograms at a representative point (140°E, 39°N) caused by the GCMT solution for the 2011 Tohoku earthquake. For the normal-mode summation, we consider both spheroidal modes, ${}_nS_l$, and toroidal modes, ${}_nT_l$, where n means the radial order number and l represents the angular order number. Fig. 6(b) exhibits the calculated seismograms when the mode summation is done for a period range longer than 4 s with several

overtones ($n \leq 8$), and only the fundamental mode without overtones ($n = 0$). We found that one spectral peak appears around 35 mHz in the overtone case. Additional experiment implied that the high overtone modes ($n = 6$–8) especially have potentials to make a peak around 35 mHz. It is unclear whether this experimental result well explains our observational result or not, but the experimental result implies that high-order radial overtones of strong seismic wave could make a peaky spectral signal in an ordinary (not local) layered structure.

Besides, we additionally state that the characteristic frequency of 38 mHz (26 s) in this study is the same frequency as an enigmatic microseism observed in the Gulf of Guinea (Oliver 1962; Shapiro *et al.* 2006). This peculiar consistency might be a key to understand the source mechanisms of the enigmatic signals.

5 CONCLUSION

We found the characteristic oscillation about 38 mHz (26 s) in Northeastern Japan that transiently appeared immediately after the 2011 Tohoku earthquake, using the H/V spectral ratio from the GNSS and the strong-motion seismometer data. We were not able to identify the locality of the characteristic peaky signal. The signal might be caused by the high-order radial overtones, which do not originate from a complex and local velocity structure, but further examination is needed.

ACKNOWLEDGEMENTS

We thank Ryoya Ikuta and Kazunori Yoshizawa for discussion. We also appreciate GSI, NGDS, the VERIPOS/APEX service, Hitz, GPS Solutions Inc. and National Research Institute for Earth Science and Disaster Prevention providing the data sets. Generic Mapping Tools (Wessel & Smith 1995) is useful to draw the maps.

REFERENCES

Asano, Y. *et al.*, 2011. Spatial distribution and focal mechanisms of aftershocks of the 2011 off the Pacific coast of Tohoku Earthquake, *Earth Planet Space,* **63,** 669–673.

Avallone, A. *et al.*, 2011. Very high rate (10 Hz) GPS seismology for moderate-magnitude earthquakes: the case of the Mw 6.3 L'Aquila (central Italy) event, *J. geophys. Res.,* **116,** B02305, doi:10.1029/2010JB007834.

Beroza, G. & Ide, S., 2011. Slow earthquakes and nonvolcanic tremor, *Annu. Rev. Earth. planet. Sci.,* **9,** 271–296.

Blackman, R.B. & Tukey, J.W., 1959. Particular Pairs of Windows, in *The Measurement of Power Spectra From the Point of View of Communications Engineering,* pp. 95–101, Dover.

Bonnefoy-Claudet, S., Cornou, C., Bard, P., Cotton, F., Moczo, P., Kristek, J. & Fah, D., 2006. H/V ratio: a tool for site effects evaluation. Results from 1-D noise simulations, *Geophys. J. Int.,* **167,** 827–837.

Clinton, J., 2004. Modern digital seismology—instrumentation, and small amplitude studies for the engineering world, *PhD thesis,* Caltech.

Dziewonski, A.M. & Anderson, D.L., 1981. Preliminary reference Earth model, *Phys. Earth. planet. Int.,* **25,** 297–356.

Elosegui, P., Davis, J.L., Oberlander, D., Baena, R. & Ekstrom, G., 2006. Accuracy of high-rate GPS for seismology, *Geophys. Res. Lett.,* **33,** L11308, doi:10.1029/2006GL026065.

Furumura, T., Takemura, S., Noguchi, S., Takemoto, T., Maeda, T., Iwai, K. & Padhy, S., 2011. Strong ground motions from the 2011 off-the Pacific-Coast-of-Tohoku, Japan ($M_w = 9.0$) earthquake obtained from a dense nationwide seismic network, *Landslides,* **8,** 333–338.

Ge, L. *et al.*, 2000. GPS seismometers with up to 20 Hz sampling rate, *Earth Planet Space,* **52,** 881–884.

Genrich, J.F. & Bock, Y., 2006. Instantaneous geodetic positioning with 10–50 Hz GPS measurements: noise characteristics and implications for monitoring networks, *J. geophys. Res.,* **111,** B03403, doi:10.1029/2005JB003617.

Geospatial Information Authority of Japan, 2011. The 2011 off the Pacific coast of Tohoku Earthquake on March 11, 2011: fault model, Available at: http://www.gsi.go.jp/cais/topic110422-index.html, last accessed 30 March 2015.

Gonzalez-Huizar, H., Velasco, A., Peng, Z. & Castro, R., 2012. Remote triggered seismicity caused by the 2011, M9.0 Tohoku-Oki, Japan earthquake, *Geophys. Res. Lett.,* **39,** L10302, doi:10.1029/2012GL051015.

Grapenthin, R. & Freymueller, J., 2011. The dynamics of a seismic wave field: Animation and analysis of kinematic GPS data recorded during the 2011 Tohoku-oki earthquake. Japan, *Geophys. Res. Lett.,* **38,** L18308, doi:10.1029/2011GL048405.

Kouba, J. & Heroux, P., 2001. GPS precise point positioning using IGS orbit products, *GPS Solut.,* **5,** 12–28.

Larson, K.M., Bodin, P. & Gomberg, J., 2003. Using 1-Hz GPS data to measure deformations caused by the Denali fault earthquake, *Science,* **300,** 1421–1424.

Masters, G., Barmine, M. & Kientz, S., 2011. *Mineos: User Manual Version* 1.0.2*,* Cal Inst of Tech.

Mitsui, Y. & Heki, K., 2012. Observation of Earth's free oscillation by dense GPS array: after the 2011 Tohoku megathrust earthquake, *Sci. Rep.,* **2,** 931, doi:10.1038/srep00931.

Mitsui, Y. & Heki, K., 2013. Scaling of early afterslip velocity and possible detection of tsunami-induced subsidence by GPS measurements immediately after the 2011 Tohoku-Oki earthquake, *Geophys. J. Int.,* **195,** 238–248.

Miyagi, T., Higaki, D., Yagi, H., Doshida, S., Chiba, N., Umemura, J. & Satoh, G., 2011. Reconnaissance report on landslide disasters in northeast Japan following the M 9 Tōhoku earthquake, *Landslides,* **8,** 339–342.

Miyazawa, M., 2011. Propagation of an earthquake triggering front from the 2011 Tohoku-Oki earthquake, *Geophys. Res. Lett.,* **38,** L23307, doi:10.1029/2011GL049795.

Nakamura, Y., 1989. A method for dynamic characteristics estimation of subsurface using microtremor on the ground surface, *Quater. Rep. Railway Tech. Res. Inst.,* **30,** 25–30.

Nakanishi, I., 1992. Rayleigh waves guided by sea-trench topography, *Geophys. Res. Lett.,* **19,** 2385–2388.

Nettles, M., Ekstrom, G. & Howard, C.K., 2011. Centroid-moment-tensor analysis of the 2011 off the Pacific coast of Tohoku Earthquake and its larger foreshocks and aftershocks, *Earth Planet Space,* **63,** 519–523.

Nishida, K. & Shiomi, K., 2012. Enigmatic very low frequency tremors beneath the Shonai Plain in northeastern Japan, *J. geophys. Res.,* **117,** B11302, doi:10.1029/2007JB005395.

Noguchi, S., Maeda, T. & Furumura, T., 2013. FDM simulation of an anomalous later phase from the Japan Trench subduction zone earthquakes, *Pure appl. Geophys.,* **170,** 95–108.

Oliver, J., 1962. A worldwide storm of microseisms with period of about 27 seconds, *Bull. seism. Soc. Am.,* **52,** 507–517.

Psimoulis, P.A., Houlie, N., Michel, C., Meindl, M. & Rothacher, M., 2014. Long-period surface motion of the multipatch Mw9.0 Tohoku-Oki earthquake, *Geophys. J. Int.,* **199,** 968–980.

Shapiro, N., Ritzwoller, M.H. & Bensen, G.D., 2006. Source location of the 26 sec microseism from cross-correlations of ambient seismic noise, *Geophys. Res. Lett.,* **331,** L18310, doi:10.1029/2006GL027010.

Singleton, R.C., 1979. Mixed radix fast Fourier transforms, in *Programs for Digital Signal Processing*, pp. 1.4-1–1.4-18, eds IEEE Digital Signal Processing Committee, IEEE Press.

Wessel, P. & Smith, W., 1995. New version of the generic mapping tools released, *EOS, Trans. Am. geophys. Un.,* **76,** 329.

Widmer-Schnidrig, R. & Laske, G., 2007. Theory and observations—normal modes and surface wave measurements, *Treatise Geophys.,* **1,** 67–125.

Yomogida, K., Okuyama, R. & Nakanishi, I., 2002. Anomalous Rayleigh-wave propagation along oceanic trench, *Stud. Geophys. Geod.,* **46,** 691–710.